Chapter 3

Determination of an Anti-HIV Drug "Nevirapine" using Electro-active 2D Materials Pd@rGO Decorated with MoS_2 Quantum Dots

3.1 Introduction

Nevirapine (NVP, 11-cyclopropyl-5, 11-dihydro-4-methyl-6H-dipyrido [3, 2-b: 20, 30-e] [1, 4] diazepin-6-one) is an anti-retroviral agent against HIV-1, which is one of the representative members of class non-nucleoside reverse transcriptase inhibitor (NNRTI) (as shown in Figure 3.1). The property of this drug is to inhibit the activities of both types of RNA and DNA dependent DNA polymerase by binding directly the catalytic site of reverse transcriptase enzyme [Rao, *et al.*, 2010; Adkins *et al.*, 1998; Hollanders *et al.*, 2000]. The advantage of NNRTI based therapy is reduction in tablet volume, more convenient administration regimen and inhibition of protease related metabolic complications. The observation of concentration of drug during first six weeks of treatment is important in patient's blood to avoid the overdose or under dose effects. Also, its high dose or prolonged use may cause various side effects like the development of rashes on the body (including hypersensitivity, Steven- Johnson syndrome and toxic epidermal necrolysis) and serious liver dysfunction which is generally originated during first six weeks of treatment [Ghosh *et al.*, 2011].

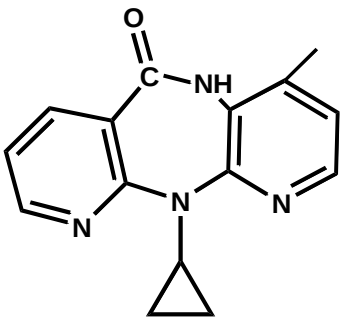

Figure 3.1 Structure of Nevirapine

Therefore, it is necessary to develop an easy and low cost method of determination of NVP in patient's blood and the side effects or occurrence of viral resistance could be delayed. This can be fruitful in maintaining optimum dose for HIV-1 infected patients and keeping NVP concentration in human blood at a low level [Hollanders *et al.*, 2000].

Literature suggests that there are various methods which have been employed for determination of NVP in human blood such as High performance liquid chromatography (HPLC) [Heeswijk *et al.*, 1998], High performance thin layer chromatography (HPTLC) [Lopez *et al.*, 2001] high performance liquid chromatography following solid phase extraction (HPLC-SPE) [Pav *et al.*, 1999], Matrix assisted laser desorption/ionization time-of-flight mass spectrometry (MALDI-TOF-MS) [Notari *et al.*, 2012] micelle electro kinetic chromatographic (MEKC) [Sekar *et al.*, 2008], capillary zone electrophoresis (CZE) [Fan *et al.*, 2002], and radio immunoassay [Rahway *et al.*,1983]. The above mentioned techniques offer high costs, time consuming and bulky pre-treatment operations which limit their use in laboratories. To overcome above issues, there is a strong need to develop simple, cost effective and sensitive sensors. Nanomaterials have unique properties like high surface area and electrochemical properties which are fruitful in improving sensing parameters such as stability, sensitivity and specificity [Tiwari *et al.*, 2016; Gupta *et al.*, 2014; Kashish *et al.*, 2015] as also discussed in the first two chapters. The same nanomaterials and modification of the sensor probes as used for AZT are tried for the detection of this drug also. However, this drug showed electro-oxidative response and the nanomaterials used for AZT are not found suitable for electro-oxidation studies due to oxidation of nano-silver above 0.2 V. Therefore, other nanomaterials were explored for this sensor.

Among the noble metal nanoparticles, palladium nanoparticles offer a variety of potential applications in sensors, energy storage, catalysis and photonics due to its high electro-catalytic properties [Lim *et al.*, 2009; Zeng *et al.*, 2011; Watt *et al.*, 2010; Sookhakiana *et al.*, 2017; Cincotto *et al.*, 2017]. The electro-catalytic properties are totally dependent on shape, size and morphology of nanoparticles which can be controlled by choosing suitable matrix [Wilson *et al.*, 2005; Pileni 2005]. 2-dimensional materials like graphene oxide (GO) can prove to be a better matrix as offers excellent catalytic properties due to larger surface area and high chemical stability. Palladium nanoparticles in GO or reduced grapheme oxide (rGO) matrixes are dispersed homogeneously (can be abbreviated as Pd@rGO) without affecting their electrical properties [Li *et al.*, 2010]. The previous studies showed that the nanostructure platform modified by Pd@rGO can prove to be a highly desirable platform for sensing purpose due to enhanced properties.

Recently, the emergence of a new class of 2D nanomaterials of transition metal dichalcogenides (TMDCs), have got much attention in scientific research [Zhuang *et al.*, 2015]. One such interesting material is molybdenum disulfide (MoS_2), which has unique properties such as excellent catalytic activity, extraordinary electrical and optical properties. The applications of MoS_2 have in various fields from energy storage to biomedical engineering [Pumera *et al.*, 2014; Xia *et al.*, 2014]. The lamellar structure of monolayer MoS_2 composed of S–Mo–S stacked three atomic layers bonded through weak Vander Waals forces. MoS_2 have some structural defects like point defects, grain boundaries and edges which play a significant role in the biomedical application. The surface modification can influence the chemical, electrical, and optical properties due to the presence of defects in MoS_2 [Carbone *et al.*, 2015; Zhou *et al.*, 2013]. However, the efficiency of sensing devices can be improved by using MoS_2 quantum dots (MoS_2

QDs) due to a large specific area and high catalytic activity which makes it an ideal platform for enhancing sensing signal. MoS_2 QDs based nanocomposite has been used in the past few years in sensing applications for improving the sensitivity, response, and stability of sensors. The nanocomposite of graphene derivative with transition metal dichalcogenides (TMDCs) [Tang *et al.*, 2014] quantum dots such as MoS_2 QDs has been explored for the applications with enhanced functional properties of each of the component via cooperative interaction. Due to the enhanced electron transfer properties of the composite modified electrode surface is one of the key factors for the development of sensitive sensing devices [Nirala *et al.*, 2015; Gong *et al.*, 2017].

In the present work, we developed a novel sensor for electrochemical determination of NVP based on Pd@rGO/ MoS_2 QDs modified glassy carbon electrodes (GCEs). We have shown an interaction between the Pd@rGO and MoS_2 QDs in the composite and based on this designed materials we showed selective and catalytic oxidation of NVP. The synergistically enhanced the electro-catalytic activity of Pd@rGO/ MoS_2 QDs composite towards the oxidation of NVP and resulted in the detection limit of NVP up to 50 nM concentration. The developed sensor showed a linear relationship between the oxidation peak current and NVP concentration in the wide range 0.1 – 80 µM under optimized conditions. Further, the proposed method is also employed for detection of NVP in complex system (human serum) samples.

3.2 Experimental section

3.2.1 Materials

Nevirapine is purchased from Sigma, Aldrich, USA. Na_2HPO_4, NaH_2PO_4, absolute ethanol, conc. HCl and distilled water are procured from Merck. India. All

chemicals utilized are of analytical grade. $PdCl_2$ and L-ascorbic acid are procured from Sigma, Aldrich. L-cysteine and Na_2MoO_4, KCl and KBr are obtained from SRL, India private limited. For all electrochemical measurements, a freshly prepared solution of Nevirapine is prepared using 1:4 ratios of ethanol and water.

3.2.2 Instrumentation

Structural and morphological measurements are executed using FEI Tecnai G2 TEM. UV-Vis. absorption studies are performed using EPOCH2 Micro plate Reader (Biotek, USA). Zeta potential is done using Nanoparticle Analyser SZ-100, Japan. IR studies are performed using FT-IR spectrophotometer (Perkin Elmer Spectrum 100, Germany). All electrochemical measurements are performed using Autolab (PGSTAT, 302, The Netherlands). GCE is used as working electrode, Ag /AgCl is used as reference electrode and Pt foil is used as counter electrode all electrochemical measurements.

3.2.3 Synthesis of Pd@rGO nanostructure

We have synthesized Pd@rGO composite using the modified method as reported by Kumar *et al.,* 2014 [Kumar *et al.,* 2014]. In brief; 5 mL (1 mg/mL) of graphene oxide aqueous suspension (synthesized in our lab) was mixed with 5 mL (10 mM) of Na_2PdCl_2 solution, and kept on stirring for 10 minutes at 50 ºC. Then, 1 mL (5 mM) of L-ascorbic acid solution was added drop wise to above solution followed by stirring for 2 h at 80 ºC. During the reaction, we have added 500 mL (1 mM) of KCl and KBr for inhibiting the agglomeration of the Pd nanoparticles. The Final precipitated product was collected by centrifugation and followed by washing with distilled water

(DI) and dried under vacuum. A Schematic diagram related to the synthesis of Pd@rGO is shown in Figure 3.2.

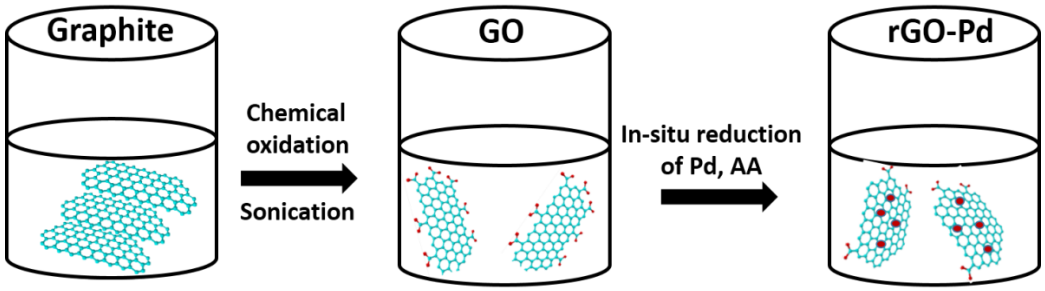

Figure 3.2 Schematic representation of Pd@rGO synthesis.

3.2.4 Synthesis of MoS_2 QDs

MoS_2 QDs were synthesized using facile, one step through hydrothermal method. In brief, 0.25 g of sodium molybdate ($Na_2MoO_4.2H_2O$) and 0.5 g of L-cysteine ($HO_2CCH\ (NH_2)\ CH_2SH$) were dissolved in 25 mL of deionized water separately. Both the solutions were kept on constant stirring for 15 minutes. After that two solutions were mixed into each other under constant stirring at ~40°C. Then concentrated HCl was used for maintaining the pH (3.0) of solution mixture. The solution is transferred into 100 mL capacity of stainless steel lined Teflon autoclave and left for 42 hours at ~190°C. After this solution naturally cools down, finally, we get a yellow colloidal solution, having MoS_2 QDs. The solution was further dialyzed through a dialysis bag (retained molecular weight 2000 Da) for 3 days to get the final product as MoS_2 QDs.

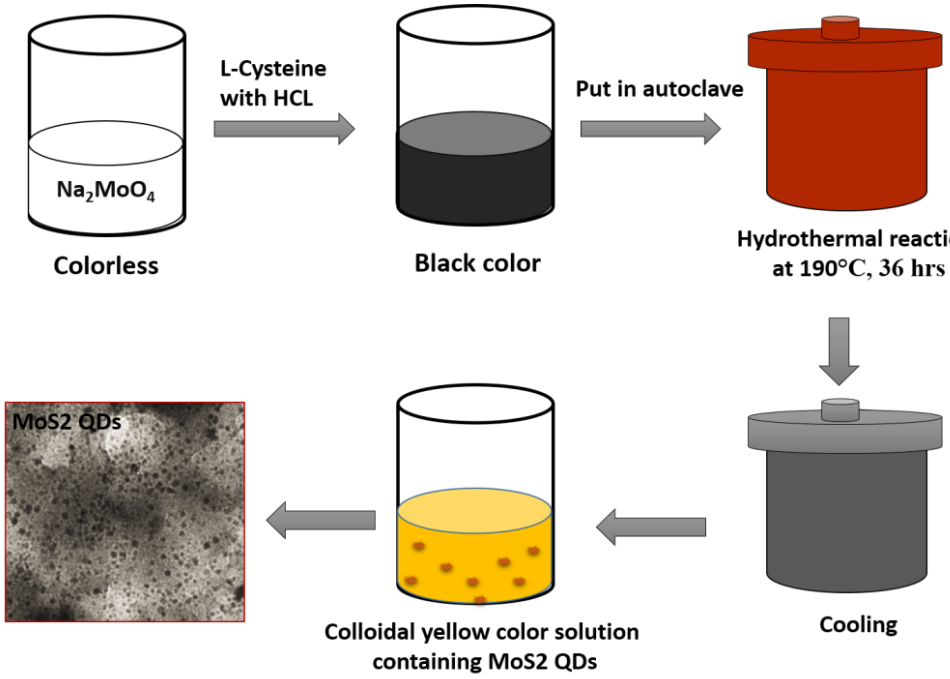

Figure 3.3 Schematic representation of MoS_2 QDs synthesis.

3.2.5 Synthesis of 2D composite (Pd@rGO/ MoS_2 QDs)

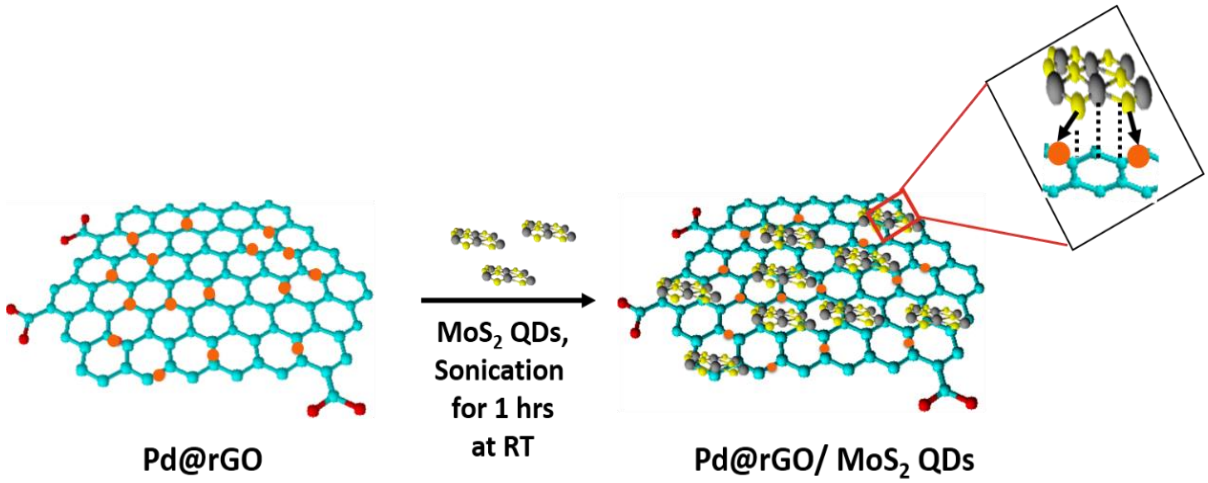

Figure 3.4 Schematic representation of 2D composite (Pd@rGO/ MoS_2 QDs) formation

Composite of Pd@rGO and MoS_2 QDs is prepared when both the individual components are mixed together in a fixed ratio by just simple mixing, and kept for 1 h under ultra-sonication. In composite, sulphur atom of MoS_2 QDs might be co-ordinately bonded to the palladium atom, and weakly bonded by Vander Waal forces of attraction to the aromatic rigs of Pd@rGO with MoS_2 QDs as shown in Figure 3.4.

3.2.6 Electrode surface modification with 2D materials

Glassy carbon electrode (GCE) of 3 mm diameter is employed for the modification for electrochemical studies. Prior to the electrode modification, cleaning of electrode surface is performed on a polishing pad using nano alumina powder and sonicated in distilled water for 10 minutes. The electrode surface is functionalized by drop casting method using aqueous suspension of Pd@rGO, MoS_2 QDs, and Pd@rGO/ MoS_2 QDs and dried under vacuum desiccator for 12 hrs. The modified electrodes are used as such for electrochemical measurements without further any processing.

3.3 Results and discussion

3.3.1 Investigation of optical properties of 2D materials

UV- Vis. absorption spectrum of Pd@rGO, MoS_2 QDs and Pd@rGO/ MoS_2 QDs has been shown in Figure. 5. Two prominent UV- Vis. absorption peaks at 267 nm and 367 nm appeared for MoS_2 QDs confirmed the excitonic features of MoS_2 QDs. Low dimensional QDs exhibit strong blue shift when the lateral dimensions of the MoS_2 nanostructures are reduced below 50 nm. In our case, as the majority of the QDs are below 50 nm, a large blue shift is expected, as also reported earlier [Jiang *et al.*, 2015]. Pd@rGO exhibits major absorption spectrum at 263 nm and 574 nm attributed to the π–π^* transition of carbon double bonds and another one due to the presence of SPR band

of palladium nanoparticles [Yang *et al.*, 2012]. The nanocomposite of Pd@rGO and MoS_2 QDs depict only two absorption peaks at 270 nm and 394 nm (weak absorption). The quenching of peaks at 263 nm and 574 nm of Pd@rGO and considerable shift MoS_2 peaks are indicating a strong interaction between both the components. The interaction between MoS_2 QDs and Pd@rGO is further investigated using FT-IR spectroscopy.

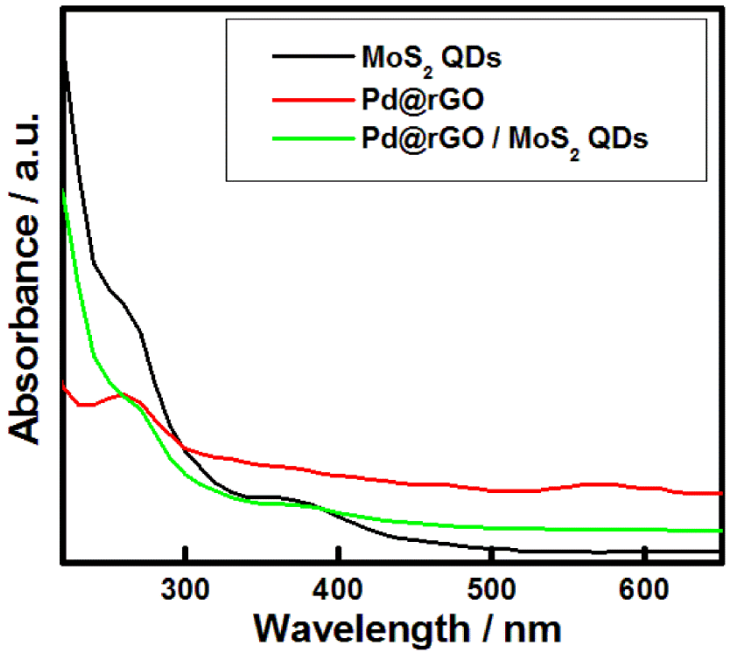

Figure 3.5 UV-Vis. Absorption spectra of 2D materials.

FT-IR Spectra of GO (a), Pd@rGO (b), MoS_2 QDs (c) and composite Pd@rGO/ MoS_2 QDs (d) have shown in Figure 3.6. The spectrum of GO exhibits major absorption frequencies at 1625 cm^{-1} corresponding to –C=C skeletal vibration, 1745 cm^{-1} and 1392 cm^{-1} due to –C=O stretching vibration frequency. The band at 1240 cm^{-1} can be due to (-C-O-C) epoxide linkages. The absorption frequencies at 3428 cm^{-1}, 1045 cm^{-1} and 782 cm^{-1} can be due to the presence of –OH functional groups. After the formation of Pd@rGO, The intensity of various absorption frequencies of GO get reduced which

indicates a partial reduction of GO into rGO. MoS_2 QDs exhibits major absorption frequencies 1613 cm^{-1} corresponding to –C=O stretching vibration due to the presence of –COOH groups. Other vibrational frequencies correspond to –OH and $–NH_2$ (1003 cm^{-1} and 3417 cm^{-1}) groups. These functional groups were supposed to be present as residue of the starting reagent materials. Pd@rGO/ MoS_2 QDs composite shows the shifting in various absorption frequencies of Pd@rGO to lower wave numbers due to quenching.

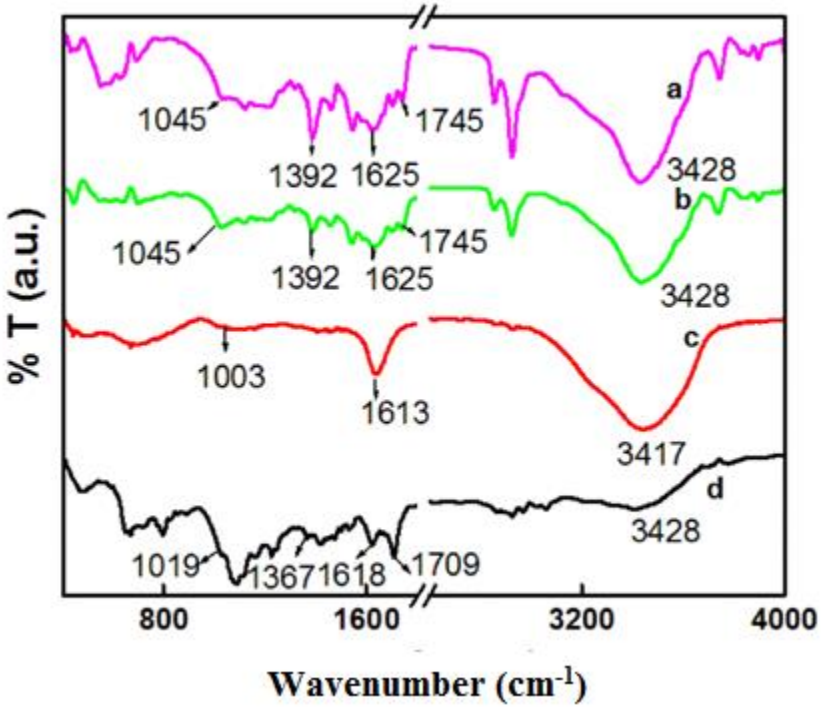

Figure 3.6 FT-IR spectra of **a**) GO **b**) Pd@rGO, **c**) MoS_2 QDs **d**) Pd@rGO/ MoS_2 QDs.

3.3.2 Structural investigation of 2D materials and its composite

Structural morphology of Pd@rGO, MoS_2 QDs, and Pd@rGO/ MoS_2 QDs was investigated by Transmission electron microscopy (TEM) as shown in Figure 3.7. In Figure 3.7a, Pd@rGO Shows palladium nanoparticles are well dispersed over reduced graphene oxide surface and (Figure 3.7b) average size distribution of Pd NPs is 5-10

nm.(Figure 3.7a, inset) The selected area electron diffraction pattern of Pd@rGO material indicates crystalline behaviour. The chemical composition of hybrid material was investigated by EDAX which confirms the presence of palladium, carbon and oxygen atoms (Figure 3.8a).

The presence of Copper is observed due to the use of carbon coated copper grid. Tem images of MoS_2 QDs (Figure 3.7c) depict narrow size distribution of monodispersed spherical nanoparticles below 10 nm which is a sign of the quantum effect. Maximum particles lie in the range of 2-6 nm as depicted in its size distribution curve. HRTEM (Inset Figure 3.7c) of MoS_2 QDs showing multilayer polycrystalline structure with interlayer spacing (0.27 nm). Its SAED pattern confirms its crystalline behaviour and EDAX confirms the presence of molybdenum and sulphur atoms in its structures (Figure 3.8b).

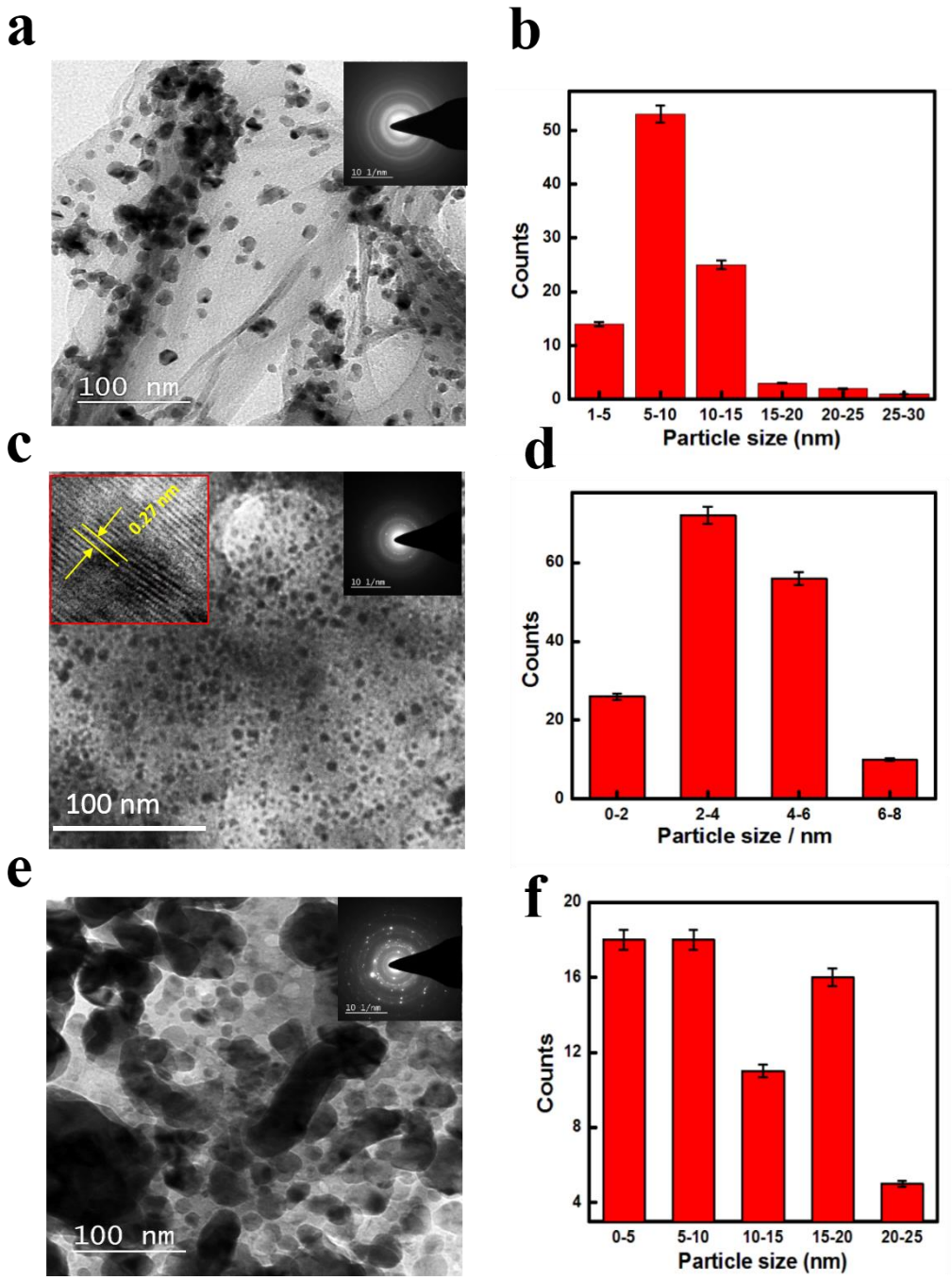

Figure 3.7 Structural investigation by TEM a) Pd@rGO (inset showing SAED pattern) b) Pd@rGO size distribution profile, c) MoS_2 QDs (inset showing its SAED pattern and interlayer spacing), d) MoS_2 QDs size distribution profile, e) Pd@rGO/ MoS_2 QDs (inset showing SAED pattern), f) its size distribution profile.

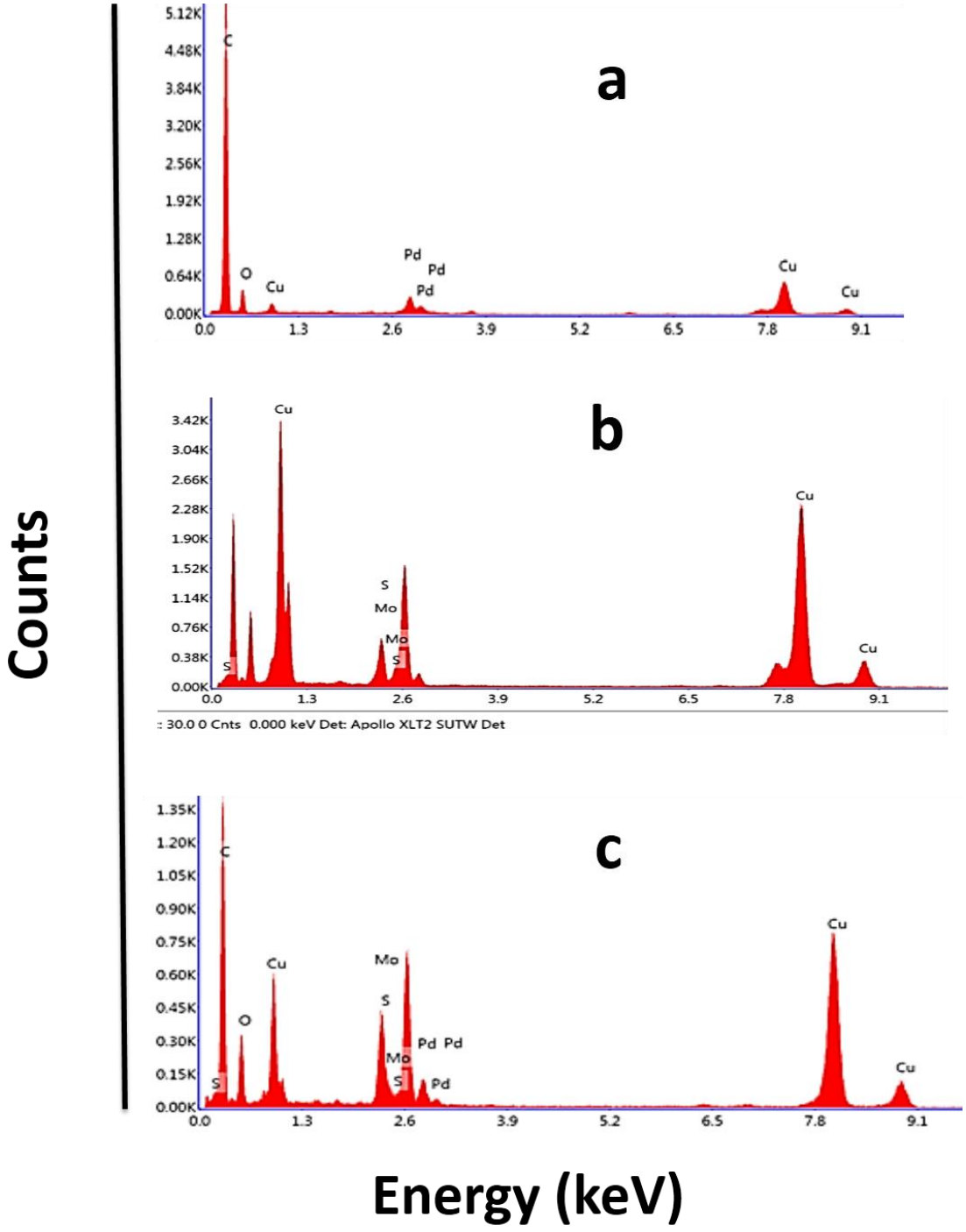

Figure 3.8 EDAX spectra of 2D materials a) Pd@rGO b) MoS_2 QDs c) Pd@rGO/ MoS_2 QDs.

Study of structural morphology of Pd@rGO/ MoS_2 QDs composite (Figure 3.7e and 3.7f) shows merging of both the nanomaterials Pd and MoS_2 QDs nicely decorated over rGO as shown in its size distribution curve. Relatively bigger sized particles are evidence of interaction of the two components. SAED pattern also confirms the crystalline behaviour of the composite. The EDAX elemental mapping of Pd@rGO/ MoS_2 QDs composite depicts the homogenous distribution of nanomaterials as shown in Figure 3.9. Elemental analysis of composite material through EDAX reveals the presence of carbon, sulphur, oxygen, palladium and molybdenum atoms in the composite (Figure 3.8c).

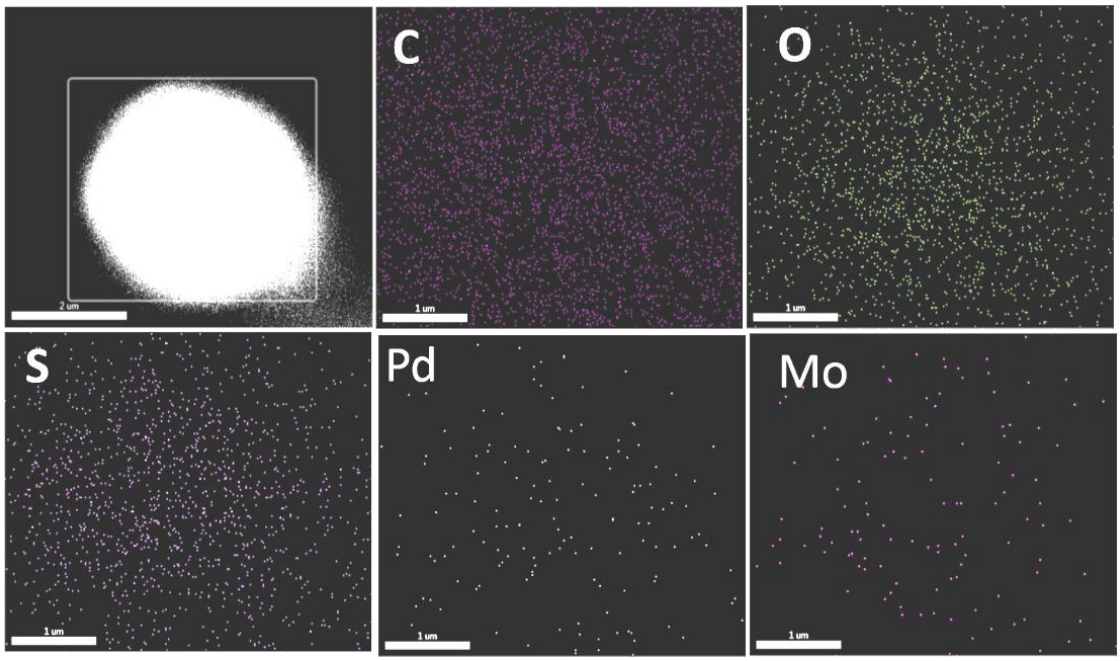

Figure 3.9 EDAX mapping of Pd@rGO/ MoS_2 QDs

3.3.3 Zeta potential measurement

Zeta potential measurement of 2D materials Pd@rGO, MoS_2QDs, Pd@rGO/ MoS_2 QDs has shown in Figure 3.10. Zeta potential of Pd@rGO is -26.1 which is almost close to MoS_2 QDs (-26.9). Zeta potential of Pd@rGO/ MoS_2QDs is -38.1 which is much greater than individual components suggesting its greater dispersibility in water due to the interaction between Pd@rGO and MoS_2QDs.

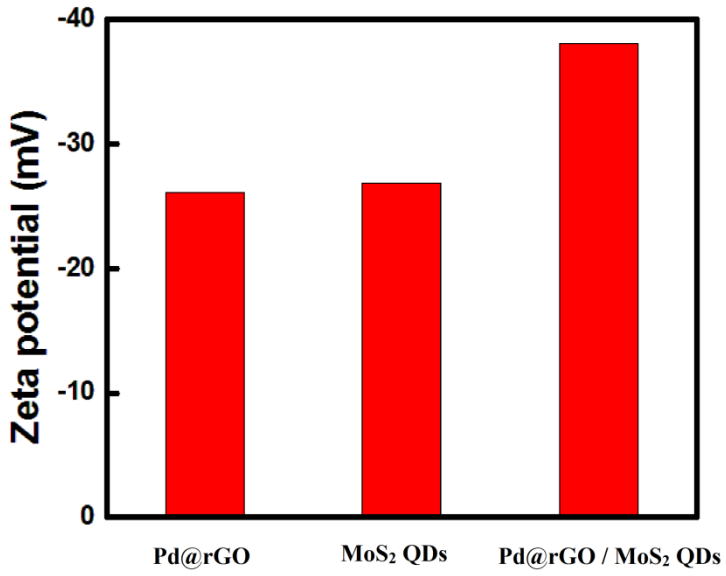

Figure 3.10 Zeta Potential measurements of 2D materials.

3.3.4 Development of modified electrodes for electro-oxidation studies

Glassy carbon electrode (GCE) of 3 mm diameter is modified with above studied materials for electrochemical studies as discussed under experimental section. The electro-oxidation of NVP is studied over the electrodes in order to develop sensitive electro-sensor for NVP. First of all, the influence of pH is checked on electro-oxidation of NVP in phosphate buffer solution as shown in Figure 3.11. It reveals that as pH of the supporting electrolyte increases, oxidation peak potential of NVP is shifted towards

less positive potential suggesting the role of protons in the electro-oxidation. When pH of the supporting electrolyte is 10 the oxidation peak potential is least positive. pH 10 is chosen with respect to lower over potential and sharp current response for electro-oxidative detection of NVP.

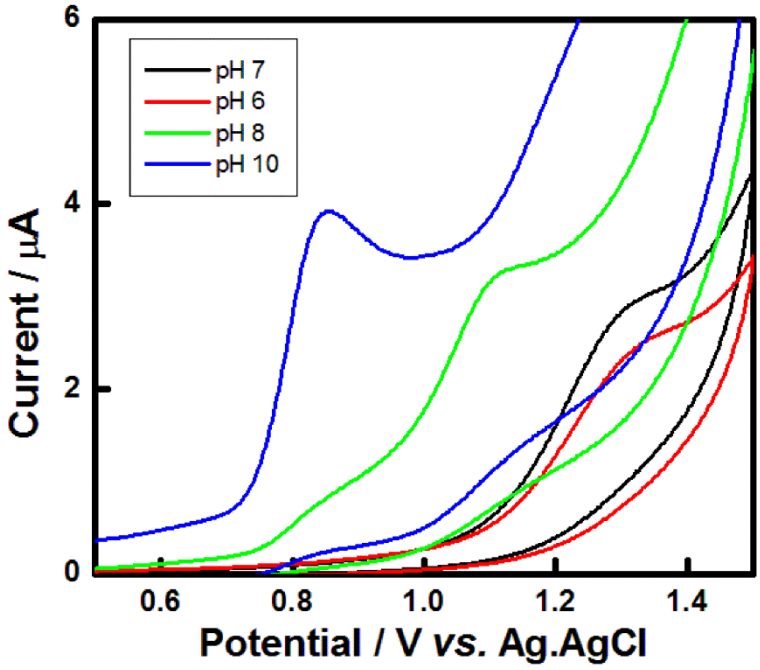

Figure 3.11 CV response of bare GCE at different pH in PBS in presence of 200 µM NVP.

To enquire the sensitivity and electro-analytical potential of as-prepared 2D materials (MoS_2 QDs, Pd@rGO, and Pd@rGO/ MoS_2 QDs), a thorough investigation has been performed using modified electrodes for electrochemical detection of NVP at a fixed concentration (27 µM) in phosphate buffer solution (pH 10). An anodic peak current corresponds to NVP electro-oxidation is obtained over all the modified electrodes as shown in Figure 3.13 with the variation of peak potential and peak current. Lowest current is observed on bare GCE at peak potential 0.85 V *vs.* Ag/AgCl. Lowest peak potential and highest peak current are observed for Pd@rGO/ MoS_2 QDs

composite modified GCE as compared to Pd@rGO and MoS_2 alone modified GCE or alone GCE. Electro-active surface area of Pd@rGO/ MoS_2 QDs composite modified electrode is calculated using Randles-Sevcik equation in presence of redox Ferri/ Ferro couple as shown in Figure 3.12.

Electro-activity of Pd@rGO/ MoS_2 QDs decorated GCE is thoroughly investigated using Fe (II)/ Fe (III) redox couple (1 mM) in PBS (pH 10, 0.1M) at a fixed scan rate of 50mV/s as shown in Figure 3.11. Pd@rGO/ MoS_2 QDs modified GCE reveals reversible behaviour of the electrode surface and enhancement of peak current by 2.5 times due to increase in electro-active surface area, electrostatic interactions between Fe (II)/ Fe (III) redox system and Mo, S and Pd atoms of the composite and fast electron transfer kinetics in between the 2D composite. Further, electro-active surface area of Pd@rGO/ MoS_2 QDs modified GCE is calculated using Randles-Sevcik equation (1)

$$i_p = 2.69 \times 10^5 \, n^{3/2} A D^{3/2} C \upsilon^{1/2} \quad \ldots\ldots\ldots (1)$$

Here, D is the diffusion coefficient of Fe (II) / Fe (III) redox couple, n is the number of electrons involved, C is the concentration of Fe (II), A is the electro-active surface area which is 0.032 cm^2 and 0.102 cm^2 for bare and the modified electrodes respectively. Modified electrode surface is almost 3 times of bare GCE.

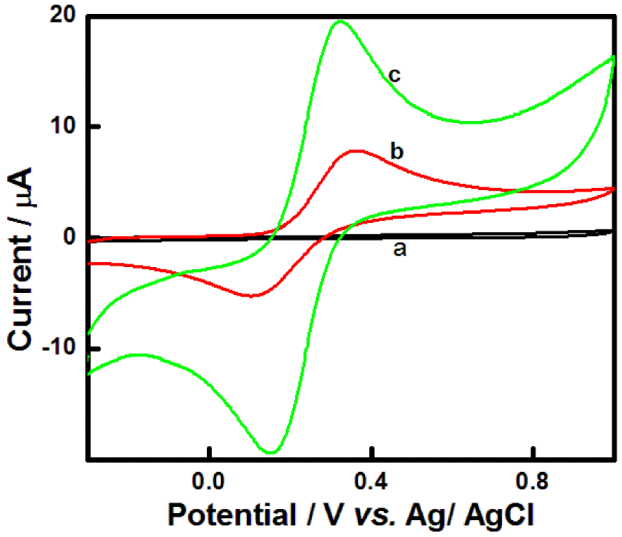

Figure 3.12 CV response of different electrode GCE in PBS (pH 10) a) GCE b) bare GCE in 1 mM $K_4[Fe(CN)_6]$ c) of Pd@rGO/ MoS_2 QDs modified GCE in 1 mM $K_4[Fe(CN)_6]$.

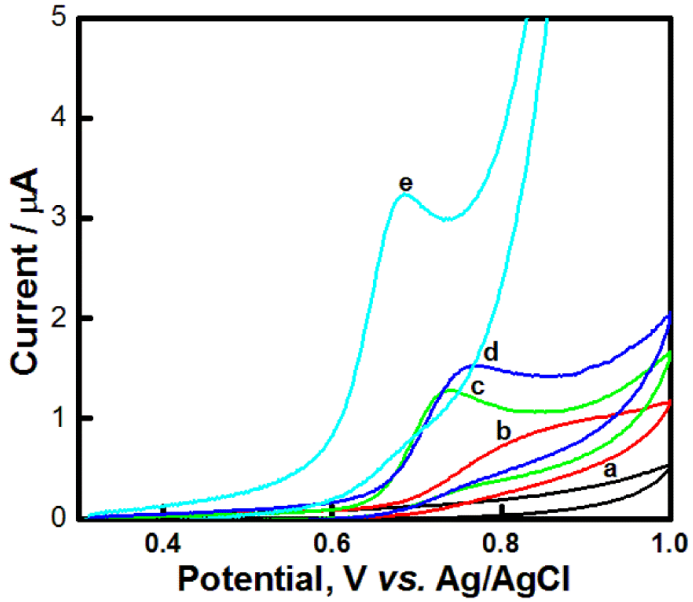

Figure 3.13 CV response of different electrodes in phosphate buffer solution (pH 10) a) bare GCE, b) Bare GCE in 27 µM NVP, c) modified MoS_2 QDs GCE in 27 µM NVP, d) modified Pd@rGO GCE in 27 µM NVP, e) Pd@rGO/ MoS_2 QDs GCE in 27 µM NVP.

3.3.5 Development of an electrochemical sensor for NVP

The modification of GCE with MoS_2 QDs, Pd@rGO and its composite i.e. Pd@rGO/ MoS_2 QDs for sensing of NVP in phosphate buffer solution at pH 10 are electrochemically characterized by CV and further DPV for estimation as discussed below.

Initially, GCE is modified with Pd@rGO for electro-oxidation studies of NVP in PBS (pH = 10). CV (Figure 3.14, I and II) and DPV techniques (Figure 3.15, I and II) are used for the study. The potential window of 0.3 V to 1.0 V *vs.* Ag/AgCl is selected for the study of electro-oxidation and estimation of NVP on the modified electrode. We observed an increasing trend of NVP oxidative peak current with increasing NVP concentration in a linear manner in the range of 0.1 µM to 80 µM due to the catalytic effect of Pd@rGO as compared to bare GCE. Similarly, GCE is modified with MoS_2 QDs in PBS (pH 10) and NVP electro-oxidation is studied through CV (Figure 3.14, III and IV) and estimated using DPV technique (Figure 3.15, III and IV). The NVP oxidation is observed in the range of 0.3 V to 1.0 V *vs.* Ag/AgCl. Under the optimised conditions a linear relationship between the oxidation peak current and drug concentration is observed in the range of 0.1 µM to 80 µM with an excellent correlation coefficient (R^2) of 0.99 as shown in Figure 3.14 III, and IV. The modified electrode shows high catalytic effect towards electro-oxidation of NVP in a wide linear range with the shift of oxidation potential at a lower potential in comparison of bare GCE and also in comparison of Pd@rGO modified GCE. A well resolved peak with a significant reduction in oxidation potential indicates better catalytic activity as compared to Pd@rGO modified electrode, however, the peak current was relatively reduced by nearly 20%. Further, the electrode was modified using both the nanomaterials.

However, rather a simple mixing we formed a composite of the two nanomaterials which was confirmed by UV-Vis. and FT-IR characterizations as discussed above.

The electrochemical response of composite Pd@rGO/ MoS_2 QDs modified GCE is studied towards electro-oxidation of NVP using CV [Figure 3.14 (V and VI)] and DPV [Figure 3.15 (V and VI)] techniques. Modified Pd@rGO/ MoS_2QDs GCE exhibits oxidation potential of NVP at 0.65 V *vs.* Ag/AgCl much lower potential than modified Pd@rGO/GCE or MoS_2 QDs/GCE. This signifies that prepared composite is more catalytic towards the electro-oxidation behaviour of NVP which can be attributed to fast electron transfer kinetics due to the synergic effect of both the individual components. Prepared sensor electrode exhibits a wide linear range of detection from 0.1 µM to 80 µM concentrations and excellent regression coefficient 0.99. The prepared sensor exhibits high sensitivity 0.037 µA/ µM and better limit of detection 50 nM through DPV and 0.094 µA/ µM and 0.1 µM through CV (Figure 3.14) at the signal to noise ratio: 3.

A possible mechanism is proposed for the electro-oxidation behaviour of NVP over the Pd@rGO/ MoS_2QDs composite modified GCE. NVP interacts with Pd@rGO/ MoS_2 QDs modified electrode due to its secondary ring nitrogen which loses an electron and forms a radical- cation which forms radical after deprotonation as shown in Figure 3.16. Then, two radicals combine and form a dimerized product. This is responsible for the anodic irreversible peak of NVP.

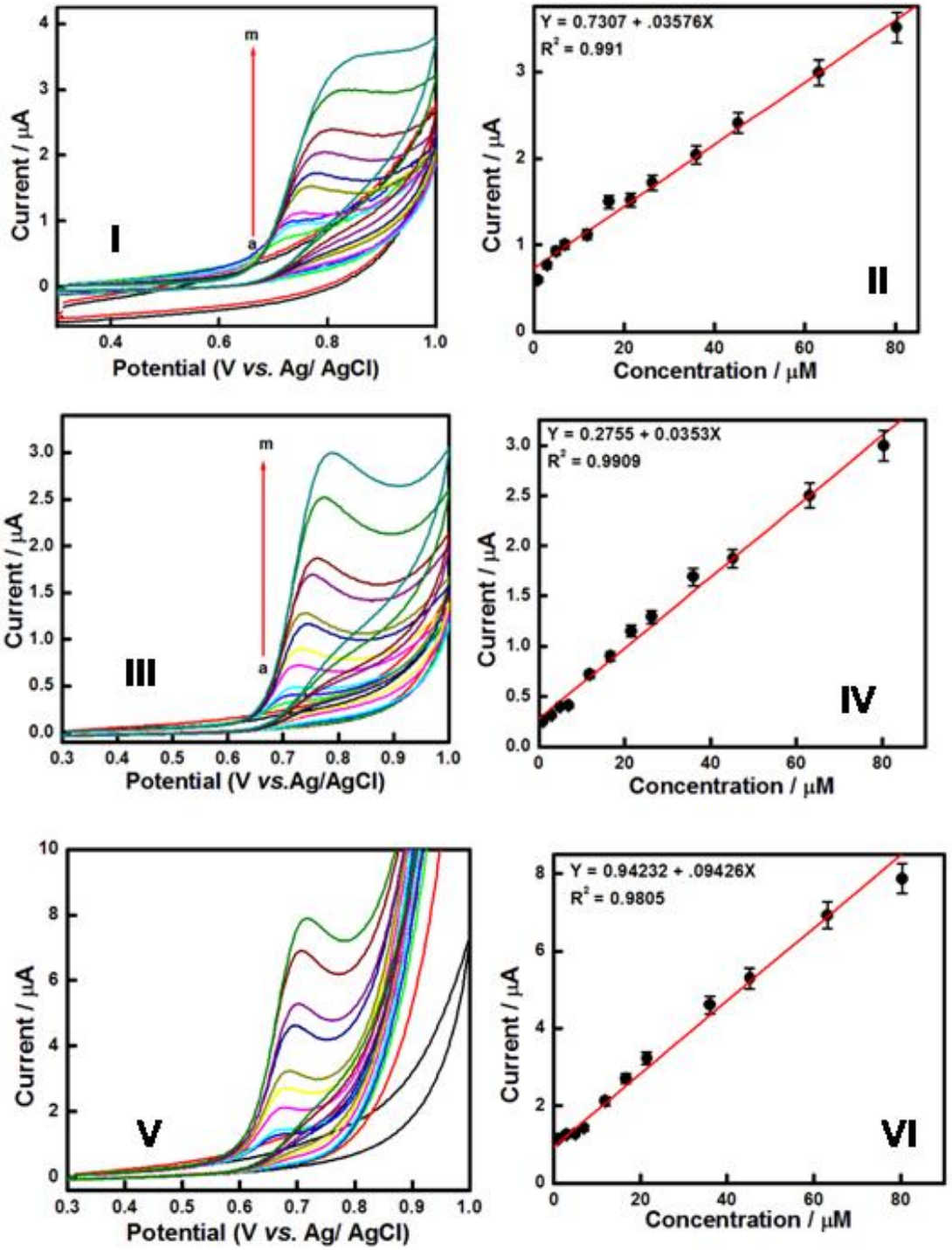

Figure 3.14 CV response of 2D materials modified GCE towards electro-oxidation of NVP from 1 µM to 80 µM concentration in PBS (pH 10, 0.1 M) I) Pd@rGO III) MoS_2 QDs V) Pd@rGO/ MoS_2 QDs composite and II, IV, VI its corresponding calibration plots.

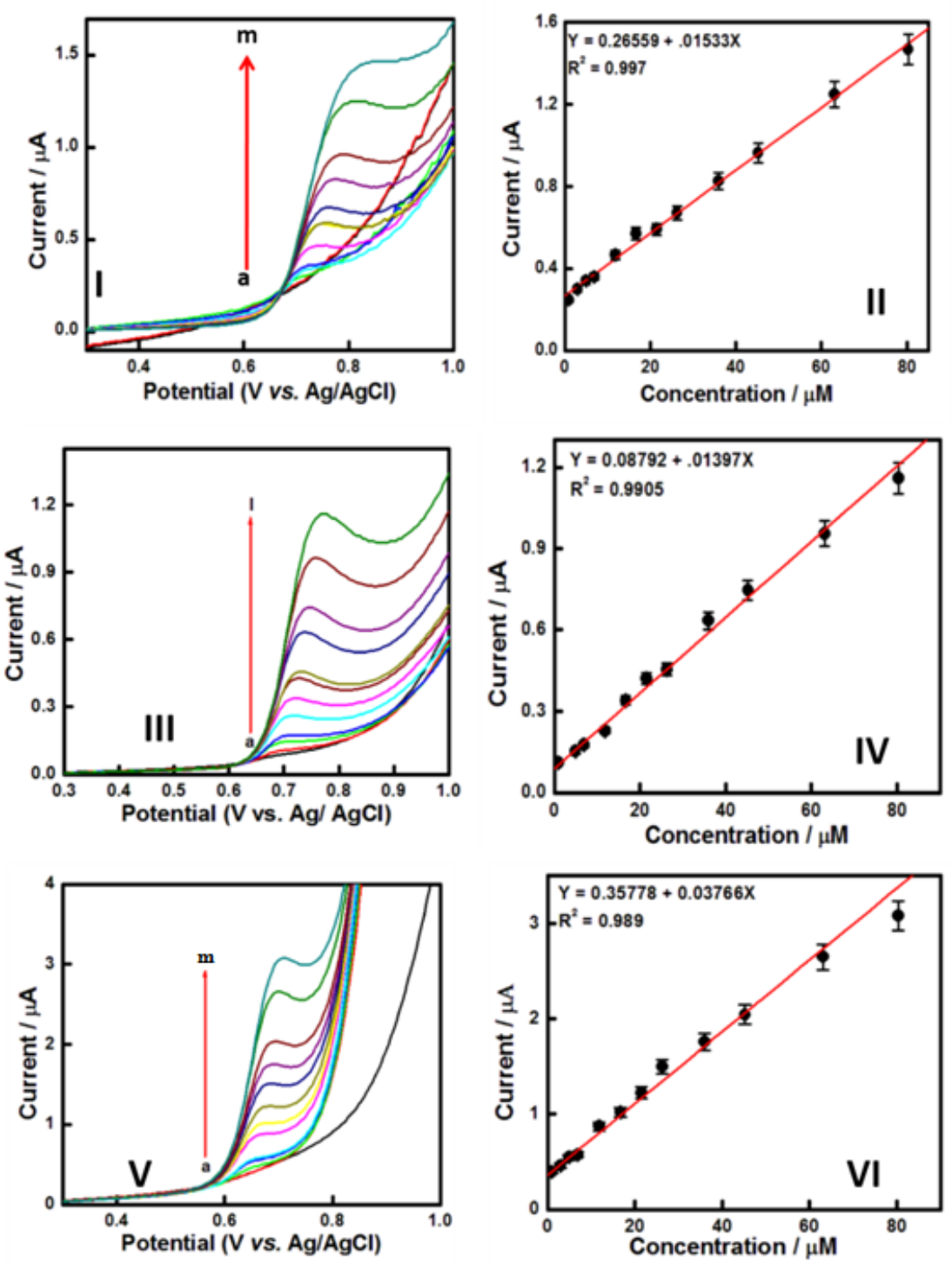

Figure 3.15 Electrochemical response of 2D composite modified electrodes for DPV a) Pd@rGO c) MoS_2 QDs e) Pd@rGO/ MoS_2 QDs in presence of NVP at different concentrations from 0.1µM to 80 µM and their corresponding calibration plot b), d), f) respectively.

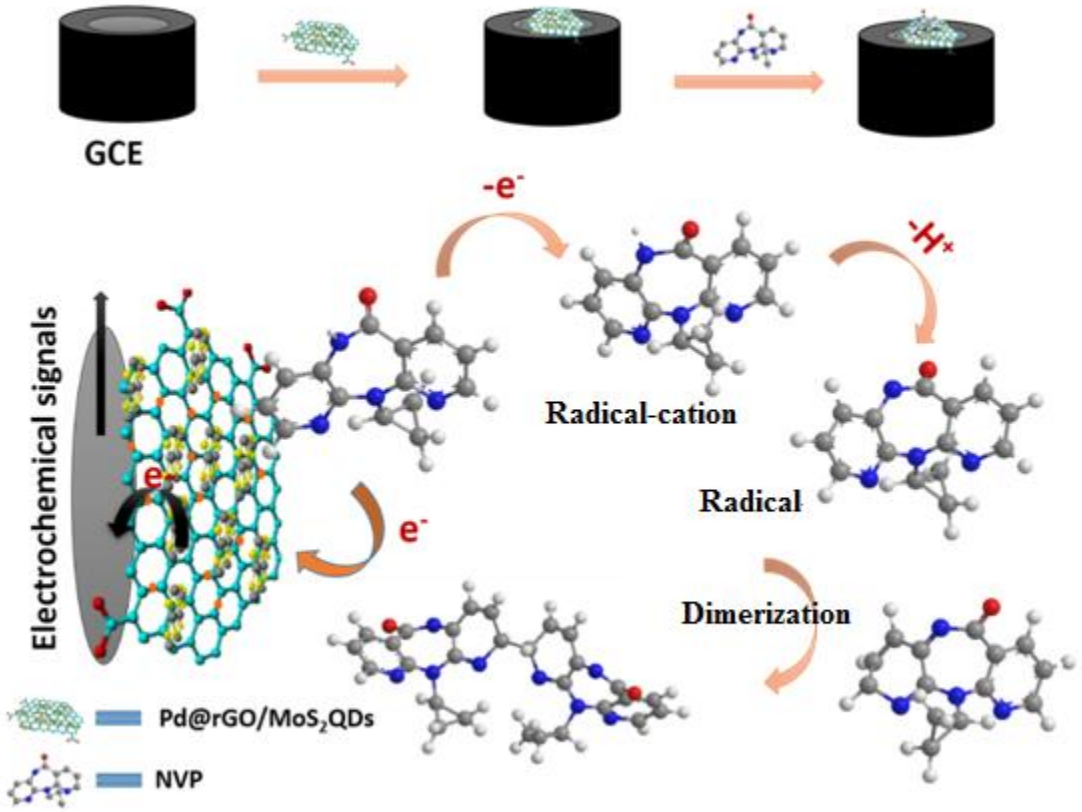

Figure 3.16 Electrode fabrication process and plausible mechanism for electro-oxidation of NVP on 2D composite modified electrode surface.

The synthesized composite material possesses a large number of sulphur and palladium atoms which provide strong electrostatic anchoring points for NVP along with palladium atoms might form a coordination bonding with nitrogen atoms of NPV. There is also the possibility of formation of hydrogen bonding between electron rich centers of NVP and electron poor centers of Pd@rGO/ MoS_2 QDs. There is a chance of formation of π-π conjugation and hydrophobic interaction between rings of Pd@rGO and aromatic rings of NVP resulting into fast electron transfer processes. The high electro-catalytic efficiency of Pd@rGO/ MoS_2 QDs facilitates the better path for electro-oxidation behaviour of NVP.

A stepwise mechanism of NVP oxidation is depicted in Figure 3.17. The plausible mechanism of NVP oxidation is in good agreement with the reported literature [Kalanur *et al.* 2010].

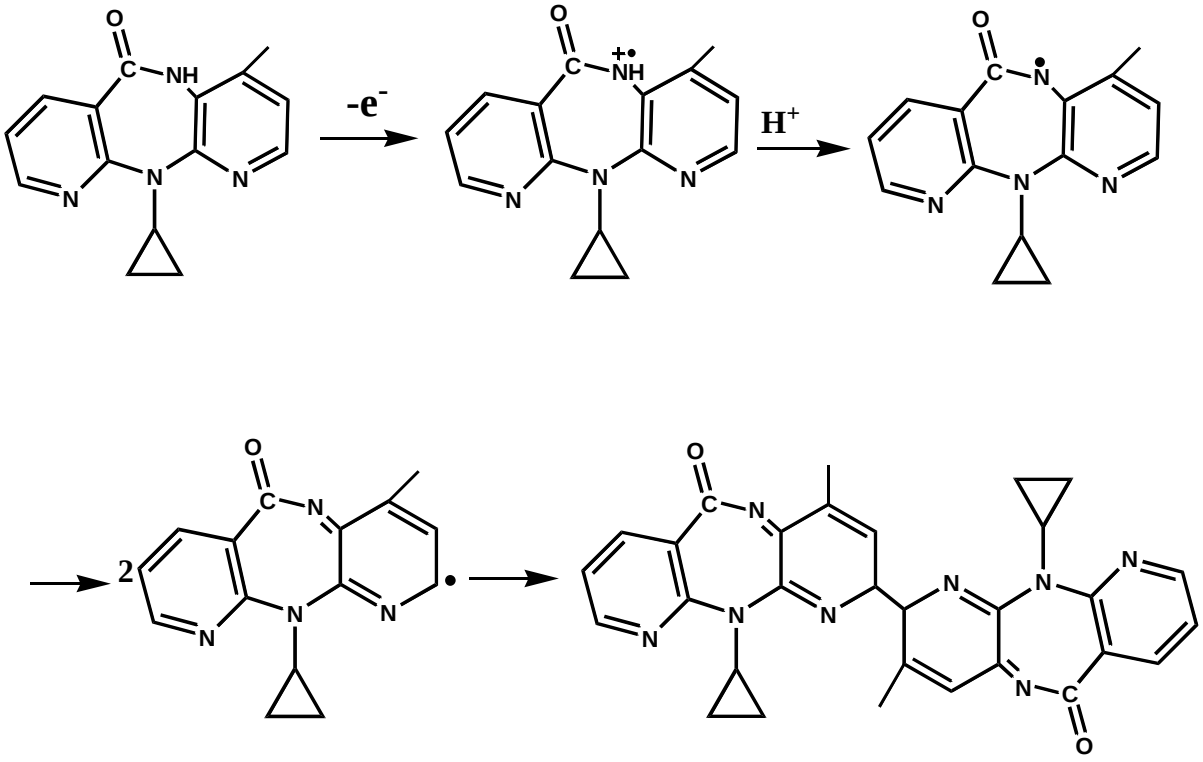

Figure 3.17 Plausible mechanisms for oxidation of NVP at pH 10.

3.3.6 Interference and practical applications

We have applied our developed electrochemical sensing platform for NVP detection by using CV (Figure 3.19) and DPV (Figure 3.18) techniques in human serum which is collected from an adult volunteer. First, we have diluted the serum sample in phosphate buffer solution (pH 10) and performed the experiments as discussed above. We observed increases in the electrochemical response of Pd@rGO/ MoS_2 QDs modified electrode in presence of different concentrations of NVP in human serum. The developed sensing platform shows good regression coefficient of 0.98 with the

detection limit of 0.1 µM from DPV studies. In human serum, another peak appears at 0.56 V which can be attributed due to the complex structural formation and matrix effect. We also checked the CV response of the composite modified GCE in real samples.

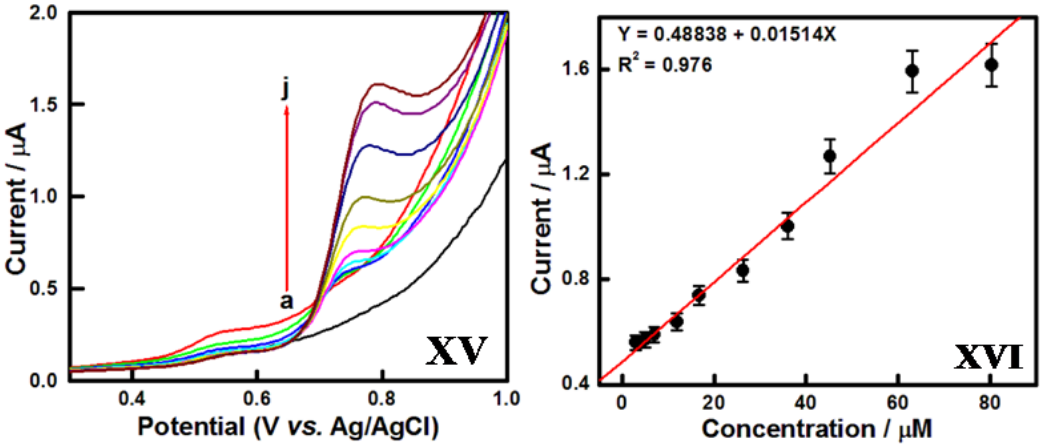

Figure 3.18 DPV response of modified Pd@rGO/ MoS_2 QDs composite GCE surface on successive addition of NVP from 5 µM to 80 µM concentration in human serum.

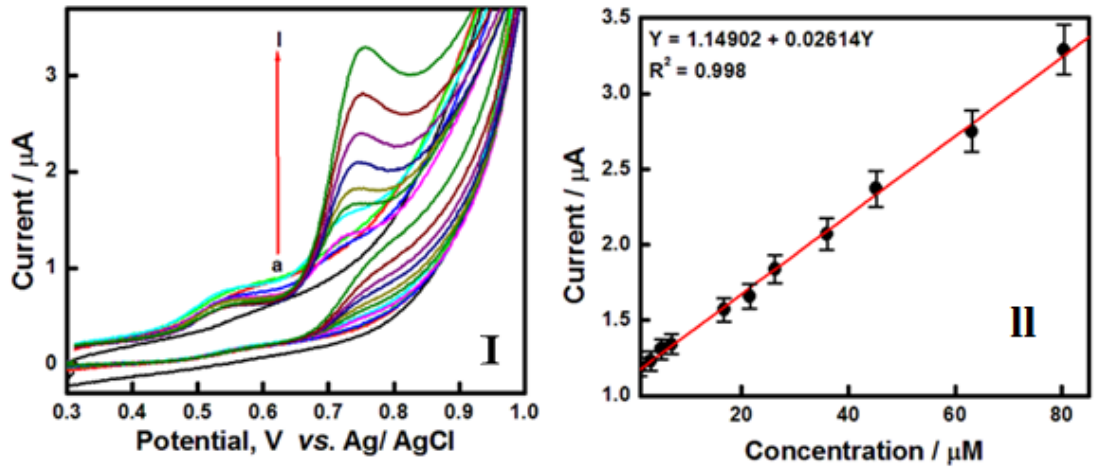

Figure 3.19 CV response of modified Pd@rGO/ MoS_2 QDs composite GCE surface on successive addition of NVP from 5 µM to 80 µM concentration in human serum.

Table 4.1 Determination of NVP in human serum

S. No.	Amount of NVP in Human Serum	Amount of NVP found (n=4)	Recovery %	Relative Standard Deviation (RSD)
1	5	4.6	92	8
2	10	9.7	97	3
3	15	15.3	102	2

n = No of Average measurements

Human serum solution is spiked with different concentration of NVP and its recovery is estimated in the complex matrix. Its relative standard deviation is found to be below 8% and its % of recovery ranges from 92 to 102 as shown in table1. This shows that Pd@rGO decorated MoS_2 QDs GCE can also be used for the estimation of NVP in clinical applications.

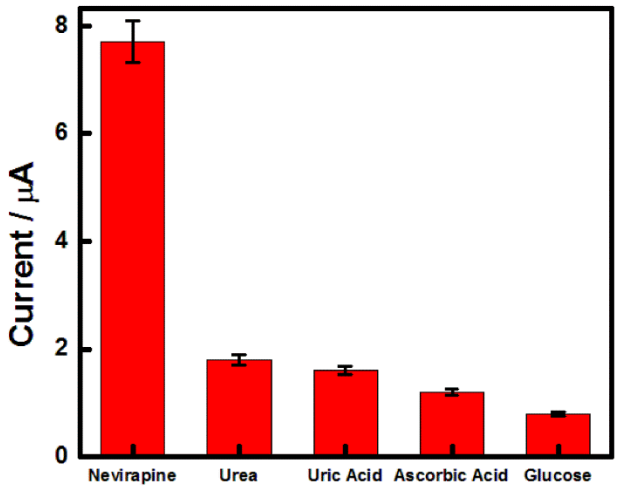

Figure 3.20 Peak current response of NVP in presence of Urea, Uric Acid, Ascorbic Acid and Glucose.

Specificity or resistance to interference is most important study that is required for use of sensors in real life complex matrixes. The electrochemical response of Pd@rGO/ MoS_2 QDs modified electrode for NVP in human serum showed no any interference due to serum matrixes but again we tried to study the interference by introducing an additional amount of some common constituents of blood. Peak current response of Pd@rGO/ MoS_2 QDs modified GCE upon addition of possible interference like Urea (0.45 mM), Uric Acid (0.5 mM), Ascorbic acid (0.4 mM) and glucose (0.5 mM) with 80 µM NVP in PBS (pH 10, 0.1M) has been studied as shown in Figure 3.20. We do not observe any significant change in current response of NVP occurs by the presence of the interfering species, which confirms that proposed sensor is specific to NVP.

Table 3.1 Comparative study for electrochemical detection of NVP based on earlier reported works.

Modified electrode	**Technique**	**Supporting electrolyte**	**Detection limit (µM)**	**Linear range (µM)**	**References**
Uracil/ CPE	DPV	0.1M NaOH	0.05	0.1-70	Zhang *et al.*, 2013
Hg/CPE	ASDPV	pH = 11.3	0.003	0.04-0.5	Mistri *et al.*, 2007
GCE	DPV	PBS pH = 10	1.03	5.0- 350	Mistri *et al.*, 2007
Au Electrode	DPV	pH = 2	-	1.1 -3.8	Ramachandran *et al.*, 2006
Bi_2O_3/ CPE	DPV	PBS pH = 8	0.110	0.05-50	Teradal *et al.*, 2015
CuO-CNP/ GCE	LSV	BR buffer pH = 7	0.066	0.1 -100	Shahrokhian *et al.*, 2015
MWCN/poly(methyleneblue)/Au	DPASV	PBS buffer pH = 11	0.05	0.1-50	Gholivand *et al.*, 2017
Pd@rGO/ MoS_2 QDs GCE	DPV	PBS pH = 10	0.05	0.1 -80	Present work

ASDPV= Anodic stripping differential pulse voltammetry, DPV= Differential pulse voltammetry, CV= Cyclic voltammetry, LSV=Linear sweep voltammetry, CPE= carbon paste electrode, GCE= Glassy carbon electrode

Further, our developed 2D nanomaterials platform has better performance to detect NVP in toxic dose range in human serum and buffer solution compared to previously reported works as described in Table 3.1.

3.4 Conclusions

In conclusion, we have studied the electrochemical response of surface modified GC electrodes with different 2D materials such as Pd@rGO, MoS_2 QDs and its composite Pd@rGO/MoS_2 QDs which facilitated fast electron transfer towards NVP electro-oxidation due to its high surface area and excellent catalytic activity. Composite modified GCE showed synergistically enhanced electro-oxidation response as compared to Pd@rGO and MoS_2 QDs alone modified GCE. The developed sensing platform was highly sensitive and displayed a linear response (0.1 µM to 80 µM concentration) with a limit of detection of 0.05 µM (50 nM) at signal-to-noise ratio (S/N): 3.Developed sensing platform showed excellent sensitivity, stability, and reproducibility. Our proposed method applied for NVP detection in real samples and observed that modified composite electrodes were highly reliable and stable for detection of NVP showing enormous potential towards portable sensing device.